Effects of density turbulence on helicon wave propagation in the core plasmas

Eun-Hwa Kim [1,2*], *Syun'ichi* Shiraiwa[1], *Seung-Hoe* Ku[1], *Alessandro* Bortolon[1], *Bart* Van Compernolle[3], *Masayuki* Ono[1], *Nicola* Bertelli[1], and *Robert* Pinsker[3]

[1] Princeton Plasma Physics Laboratory, Princeton, New Jersey, USA
[2] Andrews University, Berrien Springs, Michigan, USA
[3] General Atomics, San Diego, California, USA

Abstract. Radio frequency wave propagation can be significantly affected by density irregularities, such as filaments in the scrape-off layer or instabilities in the core plasma. In this study, we examine the impact of edge turbulence on helicon wave propagation using the Petra-M simulation tool. To analyze the effect of edge turbulence, we utilize a realistic background plasma derived from XGC simulations, which includes spatial density fluctuations at the edge. This focus is particularly relevant for the DIII-D configuration, characterized by edge density turbulence of the core plasmas in a wide pedestal QH-mode. We focus on helicon wave propagation in the core plasma since the slow mode cannot propagate into the core plasma when the density is higher than the lower hybrid resonance, where a wide pedestal QH-mode occurs. The simulation results indicate that edge density fluctuations have a substantial impact on helicon wave coupling due to scattering in the core. We specifically demonstrate that the toroidal mode number and the level of density fluctuations are significant factors influencing scattering. While we have minimized the excitation of slow modes from the antenna, we still observe mode-converted slow modes resulting from the incoming helicon waves. The insights derived from these simulations will inform upcoming tokamak experiments regarding helicon antenna coupling in long pulse scenarios.

1 Introduction

Helicon waves, also known as lower hybrid (LH) fast waves or whistler waves, are being considered for plasma heating and current drive in various tokamaks, including DIII-D [1, 2]. Recent experiments have successfully demonstrated the coupling of more than 0.7 MW of radio frequency (RF) power at 476 MHz to DIII-D plasmas through the use of a traveling wave antenna to launch helicon waves [3].

The propagation of helicon waves and parasitically excited slow waves has been numerically investigated using different full-wave simulation codes [4-6]. These waves can be significantly affected by density irregularities, such as filaments in the scrape-off layer (SOL) or instabilities in the core plasma. One study [5] focused on the effect of SOL density turbulence by employing a multi-wavelength HERMES density turbulence model [7].

In this study, we investigate the effect of edge density turbulence on helicon wave propagation in the core plasma using the Petra-M code [8, 9]. Our analysis is based on a detailed background plasma model derived from XGC simulations [10], which effectively captures the intricate spatial density fluctuations present at the plasma edge. This investigation is particularly relevant to the DIII-D configuration, known for its strong edge turbulence within the wide pedestal QH (WPQH) mode [11]. The WPQH mode represents a promising operational scenario for fusion reactors, characterized by high energy confinement without edge-localized modes, as has been successfully demonstrated in DIII-D and through numerical simulations with XGC [11].

The structure of this paper is as follows: Section 2 provides an overview of the drift wave turbulence structure obtained from XGC simulations, and Section 3 discusses full-wave simulations of helicon waves using the Petra-M code. We specifically compare the wave properties with and without the effects of density turbulence, and also examine the effect of the toroidal wavenumber of helicon waves. A summary is presented in the final section.

2 Drift Wave Turbulence from XGC

To study realistic drift-wave turbulence, we conduct a gyrokinetic simulation of DIII-D discharge #184833 at 4800ms using the XGC total-f gyrokinetic particle-in-cell code [10]. This simulation includes gyrokinetic ions and drift-kinetic electrons, along with Monte Carlo

* Corresponding author: ehkim@pppl.gov

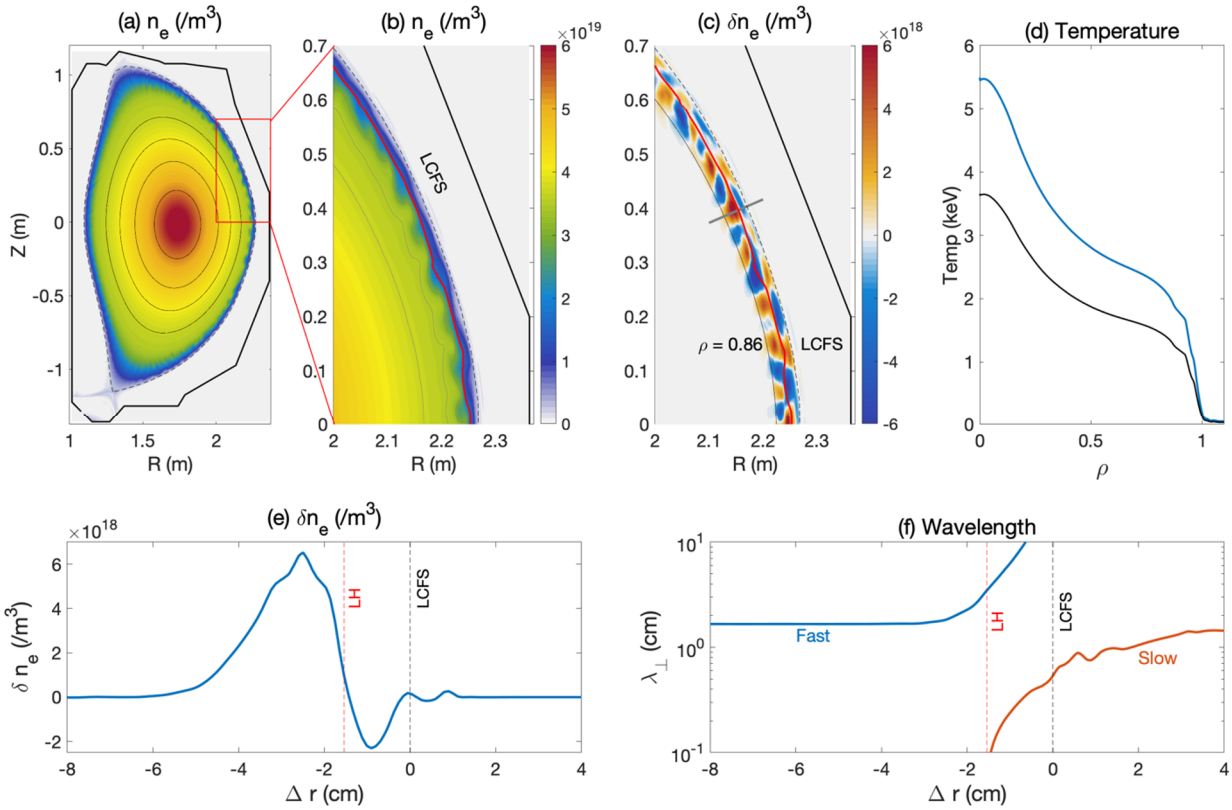

Fig. 1. (a) Electron density (n_e) constructed using XGC for DIII-D #184833 at 4800ms. Here, the thick black line represents the XGC simulation domain, and gray lines are where ρ = 0.1, 0.3, 0.5, and 0.7, respectively; (b) the n_e near the helicon antenna location, where in the red box of panel (a). Here, dashed black and red lines are the LCFS and the lower hybrid resonance location. Grey lines indicated the locations where n_e = 3.7, 3.5, and 3.0×10^{18} m^{-3}, respectively; (c) Density fluctuations (δn_e). The black dashed line is the LCFS, the thin black line is where ρ = 0.86. The grey lines is an example of quasi-perpendicular to the magnetic field line; (d) Temperature profile obtained from XGC simulation (black) and adjusted temperature profile (1.5 times higher than the original temperature) for the RF simulation (blue line) at the mid-plane, and (e) Density fluctuations are observed along the grey lines in panel (c). Here, Δr represents the distance from the LCFS, with plus and minus signs indicating directions toward the core or the SOL; and (f) Wavelengths perpendicular to the ambient magnetic field for fast (blue) and slow (orange) modes calculated by assuming a field-aligned wavenumber $n_{||}$ = 3. In panels (e) and (f), the red and black vertical lines correspond to the LH and the LCFS, respectively.

neutral particles modeled with a recycling coefficient of 0.99. We also incorporate measured carbon impurity density and electromagnetic effects. The radial pedestal profiles used as inputs for XGC are provided in Ref. [11].

To focus on electron-scale turbulence, we filter out toroidal mode numbers n=1–5 to suppress potential magnetohydrodynamic instabilities. Although these modes vary over time, the laboratory frame frequency is approximately 330 kHz, which is significantly lower than the helicon waves at 476 MHz. Therefore, for the full-wave simulations, we assume a time-stationary density profile.

Figure 1(a) presents the density fluctuation structure obtained from the XGC simulation, where density turbulence is observed along the magnetic flux surface near the edge of the plasma. In this figure, the thick black line represents the XGC simulation domain, which includes the SOL. Figure 1(b) provides a clearer perspective, showing that these fluctuations occur just inside the last closed flux surface (LCFS). The XGC density profile can be analyzed according to the poloidal mode number (m_{XGC}) of the turbulence, revealing that density turbulence in the edge plasma is minimized for m_{XGC} = 0. Consequently, we can estimate the fluctuation level as $\delta n_e = n_e - n_e (m_{XGC}=0)$. Figure 1(c) provides a detailed view of the fluctuation structure (δn_e). This analysis indicates that density turbulence predominantly occurs between ρ = 0.86 and 1, where ρ is the square root of the normalized poloidal flux. In this figure, the grey line represents a single line perpendicular to the background magnetic field, and δn_e along this line is also plotted in Figure 1(e).

The XGC code also generates a temperature profile, as shown in Figure 1(d). The peak temperature is approximately 3.5 keV, which is slightly lower than the temperatures used in previous full-wave simulations [4, 5]. For comparative purposes, we adopted a temperature profile that is 1.5 times higher than the original temperature (blue line) in the full-wave simulations.

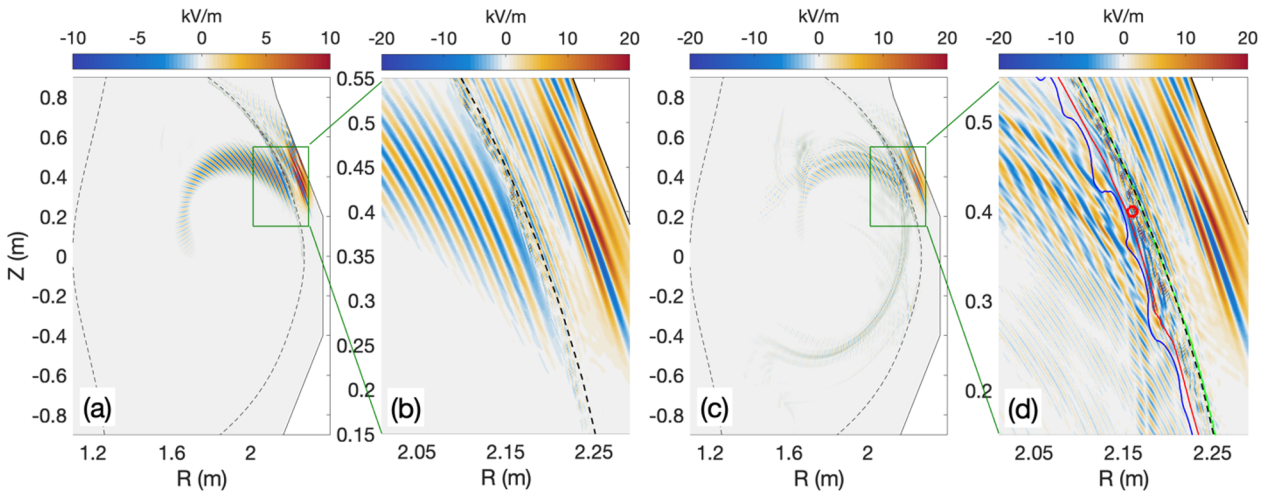

Fig. 2. Wave solution of E_r (a)-(b) without density turbulence and (c)-(d) with density turbulence. Here, panels (c) and (d) are where the magenta box in panels (a) and (c). The black dashed lines represent the LCFS; The green, red, and blue lines in (d) correspond to the helicon wave cutoff, the lower hybrid density, and the location where $n_e = 2.75 \times 10^{18}$ m^{-3} (arbitrarily chosen to show the density fluctuation structure), respectively. The red circle in panel (d) is where the wavelength perpendicular to the magnetic field has been calculated.

We calculate the wavelength perpendicular to the magnetic field along the grey line shown in Figure 1(c) for both fast and slow modes, assuming a field-aligned wavenumber of $n_{\|}$ = 3.3. The results are presented in Figure 1(f). As noted in previous studies [e.g., 1, 6], the SOL densities fall below the helicon cutoff condition, which prevents helicon waves from propagating in the SOL, making them evanescent. On the other hand, the slow mode cannot propagate in regions where the electron density is below the LH. Therefore, both wave types can co-propagate only in the region between the cutoff condition near the LCFS and the LH. In this range, we observe many density fluctuation structures in panels (c) and (e), consequently, it is anticipated that the density fluctuations in this narrow area will also influence the propagation of both slow and helicon modes.

3 Full-wave Simulations from Petra-M

Petra-M is an open-source finite element method platform built on the scalable MFEM finite element library [8, 9]. This code has been extensively utilized for plasma wave simulations in fusion devices and in the Earth's magnetosphere [12, 13].

For the simulation, we use the XGC simulation domain, as shown in Figure 2(a). The outer boundary is assumed to be a perfect reflector, representing a metal boundary. We incorporate an effective collisional damping term, following the methodologies of previous studies [6, 14]. In addition to the collisional damping, we also introduce Landau damping in the core plasma for a realistic wave absorption [4] and an artificial damping term in the SOL to eliminate unwanted slow modes. The effective collisional term can be expressed as

$$\nu = \nu_{ei} + \nu_{Landau} + \nu_{art} \ (\rho > 1),$$

where ν_{ei} is the collisional frequency between electrons and ions (from Eq. 1 in Ref. [14]), ν_{Landau} is the effective rate of Landau damping (from Eq. 105 in Ref. [15]), and ν_{art} is an additional artificial damping term. We assume that $\nu_{ei}+\nu_{art}=0.1\omega$ in the SOL.

The antenna is positioned within the SOL, with the peak wave power located at (R, Z) = (2.24, 0.4) m, similar to those in Ref. [6]. We launch waves with a frequency of 476 MHz and adopt field-aligned wavenumbers ($n_{\|}$) of 2.75, 3.3, and 3.85 (Section 3.2), as well as three different density fluctuation levels (Section 3.3).

3.1 Effect of Core Density Turbulence

We conduct simulations both with and without a density turbulence structure for $n_{\|}$=3.3. Figure 2 shows the wave solutions of the perturbed electric field in the R direction (E_r) (a)-(b) without and (c)-(d) with density turbulence. In both cases, we identify a wave mode in the SOL and another mode in the core plasma. Since helicon waves are evanescent in the SOL, the observed waves in this area are slow modes. The density in the core plasma is higher than the LH resonance density, which prevents slow modes from propagating into the core plasma. Consequently, waves in the core plasma are helicon waves.

A closer examination of the wave solutions near the LCFS in Figures 2(b) and 2(d) reveals short-wavelength waves occurring between the LCFS and the LH density. These waves occur in the regions where helicon wave power arrives, suggesting that they could be mode-converted slow modes from the helicon wave due to the abrupt increase in density [6]. One of evidence is the wavelength. As shown in Figure 1(e), the slow mode near the LH resonance has a significantly shorter wavelength compared to the helicon mode. The wavelength measured across the magnetic field line at R = 2.16 and Z = 0.4 (indicated by the red dot in Figure

2(d) and Δr = -0.1cm in Figure 1(e)) is approximately 0.2 cm, which aligns with the calculated dispersion relation. At this point, a helicon wave can also propagate; however, the calculated wavelength is about 6.2 cm.

When no density turbulence is present in Figures 2(a) and 2(b), the helicon waves propagate along a smooth ray path in the core plasma. However, when fluctuations are present in Figures 2(c) and 2(d), scattering of the helicon waves is observed. This leads to the helicon waves following multiple paths, with the main wave trajectory splitting into several routes, as shown in Figure 2(d). Additionally, the waves can propagate in the opposite direction, moving downward instead of upward. These structures are correlated to the poloidal structure of the density turbulence (blue line) as shown in Figure 2(d).

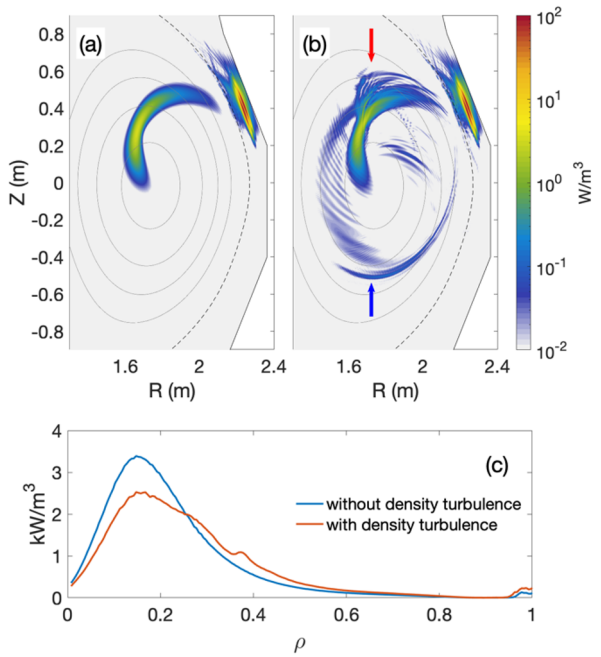

Fig. 3. Wave energy losses (**J**·**E**) (a) without and (b) with the density turbulence. The grey lines are ρ=0.1, 0.3, 0.5, and 0.7, respectively. Red and blue arrows represent the scattered helicon wave branches. (c) Energy absorption in each flux tube with (blue) and without (red) density turbulence.

We calculate the power absorption (**J**·**E**) assuming an injected power of 1 MW in the initial waves, as shown in Figure 3. Given our assumption of strong absorption in the SOL, the majority of the wave power is absorbed near the source location in the SOL as well as in the core plasma due to the helicon waves.

Without density turbulence (Figure 3(a)), it is shown that power absorption occurs mostly in the inner flux tube, $0<\rho<0.4$. However, when the density turbulence structure is present (Figure 3(b)), power is absorbed across a broader ρ within $0<\rho<0.5$. In particular, waves propagating downward (blue arrow) are evident.

The integrated energy absorption in each flux tube, as shown in Figure 3(c), clearly illustrates this effect. Here, we focus on the wave absorption in the core plasma. In both cases, maximum wave energy absorption occurs near ρ=0.15; however, the presence of density turbulence allows absorption to take place over a broader range of ρ. We observe a bump near ρ = 0.375, which is due to the scattered waves (red and blue arrows in Figure 3(b)), and a small peak near the LCFS, resulting from the mode-converted slow mode.

3.2 Effect of the Toroidal Mode Number of the Antenna

We also compare the properties of helicon waves in the core plasma for different field-aligned mode numbers ($n_{||}$ = 2.75 and 3.85) as shown in Figures 4(a) and 4(b). In these figures, stronger scattering is observed for $n_{||}$ = 2.75 in panel (a) compared to the case of $n_{||}$ = 3.85 in panel (b). Specifically, the waves propagating in the negative Z direction (blue arrow) are much more pronounced in panel (a) than in (b), and wave absorption occurs over a broad range of ρ. Consequently, the wave energy absorption plot in panel (c) shows that wave absorption for $n_{||}$ = 2.75 occurs broadly in the range of ρ, and the absorption peak near ρ = 0.35 for $n_{||}$ = 2.75 is much stronger than that for $n_{||}$ = 3.3 or 3.85.

These findings align well with previous simulation results [5], suggesting a strong correlation between wavelength and the spatial scale of turbulence in terms of helicon wave scattering and energy absorption. When the helicon wavelength is similar in size to the turbulence within the plasma, strong scattering can occur. For example, the wavelength of helicon waves at (R, Z) = (2.16, 0.4) is approximately 4.93 cm, 6.2 cm, and 7.7 cm for $n_{||}$ = 2.75, 3.3, and 3.85, respectively. As shown in Figure 1(e), the spatial scale of the density fluctuation is about 5 cm, which is close to the helicon wavelength for $n_{||}$ = 2.75.

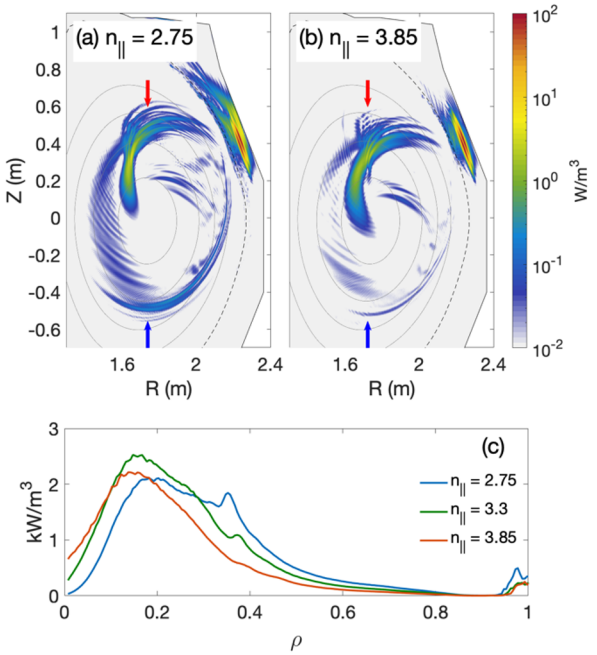

Fig. 4. Wave energy losses (**J**·**E**) for (a) $n_{||}$ = 2.75 and (b) $n_{||}$=3.85. The grey lines represent ρ = 0.1, 0.3, 0.5, and 0.7, respectively. Red and blue arrows represent the scattered helicon wave branches. Energy absorption in each flux tube (c) for $n_{||}$ = 2.75 (blue), 3.85 (red), and 3.3 (green), respectively.

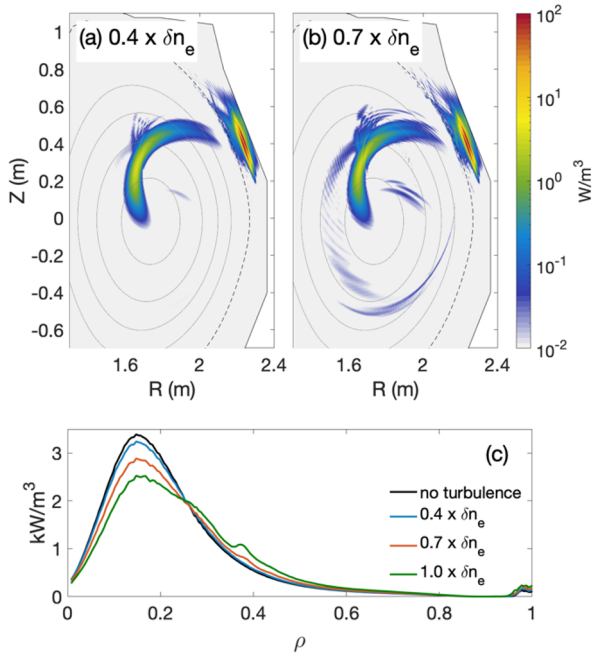

Fig. 5. Wave energy losses ($\mathbf{J}\cdot\mathbf{E}$) for (a) 0.4$\delta n_e$ and (b) 0.7 δn_e. The grey lines represent ρ = 0.1, 0.3, 0.5, and 0.7, respectively. Energy absorption in each flux tube (c) for no density turbulence (black), 0.4 δn_e (blue), 0.7δn_e (red), and δn_e (green) when $n_{||}$ = 3.3, respectively.

However, the XGC simulations incorporate multiple toroidal and poloidal mode numbers; they can not quantitatively determine the wavelength that maximizes the scattering. However, the simulation results indicate that the wavelength of the lower $n_{||}$ may be more comparable to the dominant mode number observed in the XGC simulations.

3.3 Effect of the Density Fluctuation Level

Ref. [5] indicated that the level of fluctuation in density irregularities significantly affects the absorption of helicon waves. In a similar vein, we also investigate how the level of density fluctuations affects the propagation and absorption of fast modes in the core plasma. We rescale the density fluctuation level and adopt adjusted densities, $n_e = n_e\ (m_{XGC}=0) + 0.4$ (or 0.7) δn_e.

Figure 5(a) - 5(b) presents the helicon wave power absorption in the core plasma when the density fluctuation level δn_e is reduced to 0.4 and 0.7 of the XGC density profile, respectively. For instance, the peak power loss at a density of ρ = 0.15 decreases from 3.39 × 10^3/m^3 in the case without density turbulence to 2.53 × 10^3/m^3 when density turbulence is present (representing a 25% reduction). In these cases, it is clearly demonstrated that helicon wave scattering decreases significantly as the fluctuation level diminishes, which is consistent with Ref. [5]. Therefore, a shift in power absorption toward lower flux tubes occurs, as shown in Figure 5(c). For the case of a lower density fluctuation level, the wave power absorption profile in ρ is similar to that without fluctuation.

4 Summary

We employ the XGC and Petra-M codes to conduct a thorough investigation into the impact of density turbulence on the propagation of helicon waves in the core plasma. Our analysis reveals that the spatial location of the helicon wave absorption shifts to the outer flux tubes when the fluctuation structure is taken into account.

These findings suggest that the WPQH mode can play a crucial role in preventing helicon power from penetrating the inner magnetic flux. Moreover, the extent of wave absorption seems to be influenced by the specific characteristics of the fluctuation structure and incident waves, including the toroidal mode number of helicon waves or the density fluctuation level of the WPQH mode. In addition, since the WPQH mode varies toroidally, conducting 3D simulations in the future will provide a better understanding of helicon wave propagation in the WPQH mode.

5 Acknowledgement

This material is based upon work supported by the U.S. Department of Energy, Office of Science, Office of Fusion Energy Sciences, under Award No. DE-AC20-09CH11466, using the DIII-D National Fusion Facility, a DOE Office of Science user facility, under Award No. DE-FC02-04ER54698, U.S. Department of Energy, Office of Science, Office of Advanced Scientific Computing Research and Office of Fusion Energy Sciences, Scientific Discovery through Advanced Computing (SciDAC) Program under Award No. DE-SC0024369. This research used resources of the National Energy Research Scientific Computing Center, a DOE Office of Science User Facility supported by the Office of Science of the U.S. Department of Energy under Contract No. DE-AC02-05CH11231 using NERSC Award No. FES-ERCAP0027700 and FES-ERCAP-32875. This research also used resources, via the INCITE program, of Oak Ridge Leadership Computing Facility at the Oak Ridge National Laboratory, which is supported by the Office of Science of the U.S. Department of Energy under Contract No. DE-AC05-00OR22725.

6 Disclaimer

constitute or imply its endorsement, recommendation, or favoring by the United States Government or any agency thereof. The views and opinions of authors expressed herein do not necessarily state or reflect those of the United States Government or any agency thereof.

References

1. R. I. Pinsker, Phys. Plasmas **22**, 090901 (2015). http://doi.org/10.1063/1.4930135
2. B. Van Compernolle, M.W. Brookman, C.P. Moeller, R.I. Pinsker, A.M. Garofalo, R. O'Neill, D. Geng, A. Nagy, J.P. Squire, K. Schultz et al., Nucl. Fusion **61** 116034 (2021). http://doi.org/10.1088/1741-4326/ac25c0
3. R.I. Pinsker, B. Van Compernolle, S.X. Tang, J.B. Lestz, C.P. Moeller, C.C. Petty, A. Dupuy, J.P. Squire, A.M. Garofalo, M. Porkolab et al., Nucl. Fusion **64** 126058 (2024) https://doi.org/10.1088/1741-4326/ad78e8
4. C. Lau, L A Berry, E F Jaeger, and N Bertelli, Plasma Phys. Contr. Fusion **4**, 045008 (2019). http://doi.org/10.1088/1361-6587/aafd04
5. C. Lau et al., M. Brookman, A. Dimits, B. Dudson, E. Martin, R. I. Pinsker, M. Thomas and B. Van Compernolle, Nucl. Fusion **61**, 126072 (2021). http://doi.org/10.1088/1741-4326/ac36f3
6. E.-H. Kim, M. Ono, S. Shiraiwa, N. Bertelli, M. Poulos, B. Van Compernolle, A. Bortolon, and R. I. Pinsker, Phys. Plasmas **31**, 102102 (2024). http://doi.org/10.1063/5.0222413
7. A. Dundovic, C. Evoli, D. Gaggero and D. Grasso A&A, 653, A18 (2021). https://doi.org/10.1051/0004-6361/202140801
8. S. Shiraiwa, T. Fredian, J. Hillairet, and J. Stillerman, Fusion Eng. Des. **112**, 835 (2016). http://doi.org/10.1016/j.fusengdes.2016.06.050
9. S. Shiraiwa, J. C. Wright, P. T. Bonoli, T. Kolev, and M. Stowell2, EPJ Web of Conferences **157**, 03048 (2017). http://doi.org/10.1051/epjconf/201715703048
10. S. Ku, C. S. Chang, R. Hager, R. M. Churchill, G. R. Tynan, I. Cziegler, M. Greenwald, J. Hughes, S. E. Parker, M. F. Adams, E., and P. Worley, Phys. Plasmas **25**, 056107 (2018). http://doi.org/10.1063/1.5020792
11. D. R. Ernst, A. Bortolon, C. S. Chang, S. Ku, F. Scotti, H. Q. Wang, Z. Yan, Jie Chen, C. Chrystal et al., Phys. Rev. Lett. **132**, 235102 (2024). http://doi.org/10.1103/PhysRevLett.132.235102
12. N. Bertelli, S. Shiraiwa and M. Ono, Nucl. Fusion **62** 126046 (2022). http://doi.org/10.1088/1741-4326/ac9690
13. E.-H. Kim, S. Shiraiwa, J. R. Johnson, N. Bertelli, S. K. Vines, K.-H. Kim, M. Engebretson, H. Kim, and C. O'ffill, Geophys. Res. Lett. **52**, e2024GL113368 (2025). http://doi.org/10.1029/2024GL113368
14. G. H. DeGrandchamp, W. W. Heidbrink, X. D. Du, J. B. Lestz, E.-H. Kim, S. Shiraiwa, M. A. Van Zeeland, J. A. Boedo, K. E. Thome, N. A. Crocker, and R. I. Pinsker, Phys. Plasmas **32**, 032508 (2025). http://doi.org/10.1063/5.0250878
15. F. F. Chen, Plasma Phys. Contr. Fusion **33**, 339 (1991). http://doi.org/10.1088/0741-3335/33/4/006